MODELLING ULTRASOUND IMAGING AS A LINEAR, SHIFT-VARIANT SYSTEM

J. K. H. Ng, R. W. Prager, N. G. Kingsbury,
G. M. Treece and A. H. Gee

CUED/F-INFENG/TR 509

21 January 2005

University of Cambridge
Department of Engineering
Trumpington Street
Cambridge CB2 1PZ
United Kingdom

Email: jkhn2/rwp/ngk/gmt11/ahg @eng.cam.ac.uk

Modelling Ultrasound Imaging as a Linear, Shift-Variant System

James Ng, Richard Prager, Nick Kingsbury,
Graham Treece and Andrew Gee

University of Cambridge
Department of Engineering
Trumpington Street
Cambridge CB2 1PZ

Abstract

We solve the equation that governs acoustic wave propagation in an inhomogeneous medium to show that the radio frequency ultrasound signal can be expressed as the result of filtering the tissue reflectivity by a point-spread function. We extend the analysis to make the link between the radio frequency ultrasound signal and the representation of ultrasound scatterers as small vectors with random phase in the complex plane. Others have previously performed parts of this analysis. The contribution of the present paper it to provide a single coherent treatment emphasizing the assumptions that have to be made and the physical consequences of the models derived. This leads to insights into the interaction of monopole and dipole scattering, useful techniques for simulating and analysing speckle statistics in the complex plane and a new expression for the normalised covariance of the analytic radio frequency ultrasound signal in terms of the complex envelope of the point-spread function.

1 Introduction

In this report, we demonstrate how a linear, shift-variant description of ultrasound imaging can be obtained by solving, under certain assumptions, the equation that governs wave propagation in an inhomogeneous medium. The theory of linear systems is well developed and well established in signal processing; a linear description is thus useful for casting ultrasound imaging into a framework that is well understood and for which mathematical tools already exist.

We then convert our linear model to complex analytic representation and derive the standard result whereby speckle is viewed as the result of constructive and destructive interference while forming the sum of a large number of small vectors in the complex plane. From this, the first and second order statistics of fully developed speckle can be derived.

A number of other authors have published work in this area. The paper by Gore and Leeman [7] is one of the first publications to have developed a realistic model for ultrasonic backscattering in human tissue by assuming weak scattering and a windowed monochromatic separable incident pulse. A more thorough analysis was carried out by Jensen [9] who derived the wave equation from

first principles and solved it to obtain an analytic expression for the backscattered radio-frequency (RF) trace in the time domain. Zemp *et al.* [21] provided an overview of the solution of the wave equation and extended the linear model further to the computation of signal statistics.

Our analysis here is similar to the treatments by Gore and Leeman [7] and by Jensen [9]. Like Jensen, our aim is to express the backscattered RF trace as the result of linearly filtering a map of the acoustic inhomogeneities in the imaged region by a transfer function determined by the geometry and mechanics of the ultrasonic transceiving probe. However, we have taken the extra step of proving, for the special case of a rectangular imaging setup, that the point-spread function (PSF) of the imaging system is shift-variant only in the axial direction. For the sake of clarity, all mathematical working has been deliberately presented in some detail. We have also ensured that all assumptions made are explicitly stated so that the limits on the model's validity are clearly identified.

Many authors use a complex model for the analysis of speckle [3, 17, 19, 20], relying on an analogy with the theory of laser speckle for justification [6]. We are not aware of an explicit presentation of the link between the RF ultrasound signal and its representation in the complex plane. This is therefore covered in some detail in the present paper to show the assumptions on which it is based and the relationships between the complex quantities and their analogues in the real world.

2 Background

Conventional ultrasound imaging interrogates a medium with high frequency band-limited acoustic waves and detects echoes scattered by inhomogeneities (also referred to as *scatterers*) within the medium. A single probe placed in contact with the subject is used for both the generation of these waves and the reception of their echoes. On the contact surface of a typical probe is found an array of piezoelectric crystals (referred to as the *aperture*), each of which behaves as an electromechanical transducer. At transmission, a subset of adjacent crystals, referred to as the *active aperture*, are excited coherently to produce a focussed beam. At reception, these same crystals detect the scattered echoes which are summed up coherently to yield a single RF voltage trace. Multiple RF traces are acquired by moving the centre of the active aperture and repeating this process; by lining up these individual traces next to each other in image space, an RF image is formed.

At each transmission, the emitted wave propagating through the medium gives rise to an *incident pressure field*, and the scattered waves give rise to a *scattered pressure field*. It can be shown that, at any moment in time, the total pressure field is the sum of these two fields (see section 3.1). At reception, each piezoelectric crystal in the active aperture detects the scattered pressure field and the resulting RF voltage trace is effectively obtained by summing the scattered pressure field over the surface of the active aperture and filtering this sum by the electromechanical impulse response of the crystals [2, 9, 21].

3 The Wave Equation

With the physical description of the previous section in mind, we shall proceed in this section to develop mathematical expressions for the incident pressure field and the scattered pressure field. Our analysis necessarily begins by considering the partial differential equation (PDE) that describes the propagation of acoustic waves in a non-uniform medium. We shall use the wave equation that is found in [7] and [12, chapter 8], in which the acoustic properties of the medium are specified in terms of its density and adiabatic compressibility. We shall complete our analysis by expressing the RF image as a function of time and the location of the active aperture's centre.

Our analysis assumes that there is one fixed focal point, identical for both transmission and reception. We shall also restrict ourselves to the case of weak scattering, where the energy of the scattered waves is much less than the energy of the incident waves.

To simplify the mathematics, the wave equation and its solution will be expressed in terms of angular frequency ω instead of time t; although less intuitive, this representation has the advantage of improving notational clarity by reducing convolutions in the time domain to multiplications in the frequency domain. The vector $\mathbf{x}$ will be used to represent the coordinates (x, y, z) of three-dimensional space. (A complete list of symbols is given at the end of the paper).

3.1 The Total Pressure Field

In the absence of any scatterers, we consider our medium to be uniform with density ρ_o and adiabatic compressibility κ_0. The speed c_0 at which acoustic waves travel in this uniform medium is given by [12, p. 233]

$$c_0 = \frac{1}{\sqrt{\rho_0 \kappa_0}} \tag{1}$$

The presence of scatterers in the medium may be modelled by adding spatially dependent terms $\Delta\rho(\mathbf{x})$ and $\Delta\kappa(\mathbf{x})$ to the density and the compressibility respectively. Without proof, we state that the total pressure field $P'(\mathbf{x}, \omega)$ that develops as a result of acoustic wave propagation obeys the linear PDE [7, 12]

$$\nabla^2 P'(\mathbf{x}, \omega) + \left(\frac{\omega}{c_0}\right)^2 P'(\mathbf{x}, \omega) = -(\mathbf{S}P')(\mathbf{x}, \omega) \tag{2}$$

where $\mathbf{S}$ is the *scattering operator* defined as

$$\mathbf{S} \equiv \gamma(\mathbf{x}) \left(\frac{\omega}{c_0}\right)^2 - \nabla \cdot \mu(\mathbf{x}) \nabla \tag{3}$$

and the scattering terms $\gamma(\mathbf{x})$ and $\mu(\mathbf{x})$ are defined as

$$\gamma(\mathbf{x}) \equiv \frac{\Delta\kappa(\mathbf{x})}{\kappa_0}, \ \mu(\mathbf{x}) \equiv \frac{\Delta\rho(\mathbf{x})}{\rho_0 + \Delta\rho(\mathbf{x})} \tag{4}$$

In keeping with the definitions introduced by Andersen and Trahey [2], the term $\gamma(\mathbf{x})$ contributes *monopole radiation* and $\mu(\mathbf{x})$ contributes *dipole radiation.*

Although equation 2 is, strictly speaking, homogeneous (there are no terms independent of $P'(\mathbf{x}, \omega)$), we shall nevertheless treat it as an inhomogeneous PDE and treat the non-zero right-hand-side (RHS) as a source term. This is acceptable since, in a sense, the RHS represents the source of scattered sound [12].

Since equation 2 is linear, we can write its general solution as the sum of the solution to the corresponding 'homogeneous' equation (i.e. with the RHS set to zero) and any particular solution [4, p. 2]. Denoting the solution to the 'homogeneous' equation as $P_i(\mathbf{x}, \omega)$ and the particular solution as $P_s(\mathbf{x}, \omega)$, we can therefore write the total field as

$$P'(\mathbf{x}, \omega) = P_i(\mathbf{x}, \omega) + P_s(\mathbf{x}, \omega) \tag{5}$$

To assign a physical interpretation to $P_i(\mathbf{x}, \omega)$, we observe that by setting the RHS of equation 2 to zero, we have effectively set $\Delta\rho(\mathbf{x}) = \Delta\kappa(\mathbf{x}) = 0$. We see then that $P_i(\mathbf{x}, \omega)$ is the pressure field that develops in the absence of any scatterers which, by definition, is the incident pressure field. We also know that the scattered pressure field must obey equation 2, and so we can assign our particular solution $P_s(\mathbf{x}, \omega)$ to be the scattered pressure field. With these physical interpretations for $P_i(\mathbf{x}, \omega)$ and $P_s(\mathbf{x}, \omega)$, we see that equation 5 confirms the statement in section 2 that the total pressure field is the sum of the incident pressure field and the scattered pressure field.

3.2 The Incident Pressure Field

Calculating the incident pressure field requires knowledge of the mechanics and geometry of the probe. We adopt the generalised three-dimensional coordinate system shown in Figure 1, where:

- $\mathcal{A}$ represents the surface of the active aperture.
- $\mathbf{x_0}$ is the location of the centre of $\mathcal{A}$.
- $\mathbf{x_a}$ is an arbitrary point on $\mathcal{A}$.
- $\mathcal{V}$ is a volume within which the scatterers being considered are contained.
- $\mathbf{x}'$ is an arbitrary point in $\mathcal{V}$.

The surface $\mathcal{A}$ may be considered to consist of infinitesimally small area elements $d^2\mathbf{x_a}$, each of which behaves as a simple point source mounted on a rigid baffle. The *Huygen-Fresnel principle* states that each area element contributes a spherically expanding wave to the incident pressure field [2]. The incident pressure field may therefore be obtained by summing the spherical wave contribution from each area element.

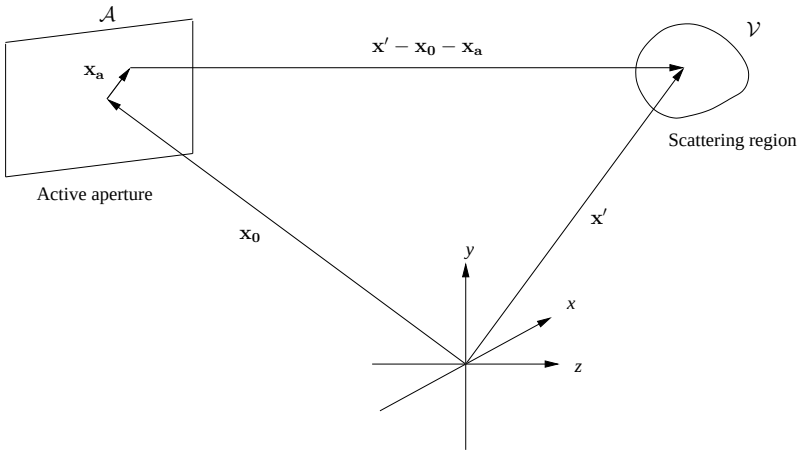

Figure 1: Coordinate system for describing scattering in an inhomogeneous medium.

If we assume that the radius of curvature of $\mathcal{A}$ is large enough that $\mathcal{A}$ may be considered to be effectively flat, then we can express the incident pressure field as the *Rayleigh integral* [8, 9, 12, 13],

$$P_i\left(\mathbf{x}, \mathbf{x_0}, \omega\right) = \frac{\rho_0}{2\pi} \int_{\mathcal{A}} j\omega V\left(\mathbf{x_a}, \omega\right) \frac{e^{-j\frac{\omega}{c_0}|\mathbf{x}-\mathbf{x_0}-\mathbf{x_a}|}}{|\mathbf{x}-\mathbf{x_0}-\mathbf{x_a}|}\, d^2\mathbf{x_a} \tag{6}$$

where $V\left(\mathbf{x_a}, \omega\right)$ is the temporal Fourier transform of the normal velocity on the active aperture's surface; this normal velocity is not uniform but varies from point to point on $\mathcal{A}$. We note that the term $j\omega V\left(\mathbf{x_a}, \omega\right)$ corresponds to the normal acceleration in the time domain, since the factor $j\omega$ corresponds to time differentiation. We have written in the argument $\mathbf{x_0}$ on the left-hand side of equation 6 to indicate explicitly the dependence of the incident pressure field on the location of the active aperture's centre.

Although we have stated equation 6 without proof, we can intuitively see that it is indeed the Huygen-Fresnel principle expressed mathematically: the integral on the RHS describes the summation of complex-valued spherically expanding waves, each weighted by the normal acceleration at its source and decaying in amplitude with increasing distance from its source.

For a typical probe, we can represent the active aperture as having a nominal normal velocity $V_n\left(\omega\right)$ weighted by a spatially varying term $a_p\left(\mathbf{x_a}\right)$ to account for apodisation. We can also model focussing by considering the normal velocity at each $\mathbf{x_a}$ to be delayed by $\tau_d\left(\mathbf{x_a}\right)$; in the temporal frequency domain, this corresponds to multiplying the normal velocity by $e^{-j\omega\tau_d(\mathbf{x_a})}$. Substituting $V\left(\mathbf{x_a}, \omega\right) = a_p\left(\mathbf{x_a}\right) V_n\left(\omega\right) e^{-j\omega\tau_d(\mathbf{x_a})}$ into equation 6, we obtain [21]

$$P_i\left(\mathbf{x}, \mathbf{x_0}, \omega\right) = \frac{j\omega\rho_0 V_n\left(\omega\right)}{2\pi} \int_{\mathcal{A}} a_p\left(\mathbf{x_a}\right) e^{-j\omega\tau_d(\mathbf{x_a})} \frac{e^{-j\frac{\omega}{c_0}|\mathbf{x}-\mathbf{x_0}-\mathbf{x_a}|}}{|\mathbf{x}-\mathbf{x_0}-\mathbf{x_a}|}\, d^2\mathbf{x_a} \tag{7}$$

For convenience, we define a new quantity $H_s\left(\mathbf{x}, \omega\right)$, which we refer to as the *spatial transfer function*,

$$H_s\left(\mathbf{x}, \omega\right) \equiv \frac{1}{2\pi} \int_{\mathcal{A}} a_p\left(\mathbf{x_a}\right) e^{-j\omega\tau_d(\mathbf{x_a})} \frac{e^{-j\frac{\omega}{c_0}|\mathbf{x}-\mathbf{x_a}|}}{|\mathbf{x}-\mathbf{x_a}|}\, d^2\mathbf{x_a} \tag{8}$$

Equation 7 can then be expressed more compactly as

$$P_i\left(\mathbf{x}, \mathbf{x_0}, \omega\right) = j\omega\rho_0 V_n\left(\omega\right) H_s\left(\mathbf{x} - \mathbf{x_0}, \omega\right) \tag{9}$$

This compact expression allows us to view the incident pressure field as the result of temporally filtering the nominal normal velocity $V_n\left(\omega\right)$ by the spatial transfer function $H_s\left(\mathbf{x} - \mathbf{x_0}, \omega\right)$. We see that the spatial transfer function $H_s\left(\mathbf{x} - \mathbf{x_0}, \omega\right)$, in which is incorporated the effects of apodisation and focussing, accounts entirely for the spatial distribution of the incident pressure field.

3.3 The Scattered Pressure Field

To calculate the scattered pressure field, we solve equation 2 by using the Green's function method. We consider the waves scattered from the volume $\mathcal{V}$ to be propagating into an effectively unbounded medium, in which case the Green's function takes the form $\frac{-1}{4\pi\left|\mathbf{x}-\mathbf{x}'\right|}\exp\left(-j\frac{\omega}{c_0}\left|\mathbf{x}-\mathbf{x}'\right|\right)$ [22, pp. 121–138]. The particular solution to equation 2 is then the product of the RHS and the Green's function integrated over the volume $\mathcal{V}$ [7, 12, 22]. Furthermore, if we define $\Delta\rho\left(\mathbf{x}\right)$ and $\Delta\kappa\left(\mathbf{x}\right)$ to be zero outside $\mathcal{V}$, then we can perform the integration over all of three-dimensional space and the scattered pressure field can be expressed as the convolution integral,

$$P_s\left(\mathbf{x}, \mathbf{x_0}, \omega\right) = \int_{\mathbb{R}^3} \left(\mathbf{S}P'\right)\left(\mathbf{x}', \mathbf{x_0}, \omega\right) \frac{e^{-j\frac{\omega}{c_0}\left|\mathbf{x}-\mathbf{x}'\right|}}{4\pi\left|\mathbf{x}-\mathbf{x}'\right|}\, d^3\mathbf{x}' \tag{10}$$

Since we are only dealing with the case of weak scattering, we assume that $\left|P_s\left(\mathbf{x}, \mathbf{x_0}, \omega\right)\right| \ll \left|P_i\left(\mathbf{x}, \mathbf{x_0}, \omega\right)\right|$. $P_s\left(\mathbf{x}, \mathbf{x_0}, \omega\right)$ in equation 5 then becomes negligible and $P'\left(\mathbf{x}, \mathbf{x_0}, \omega\right) \approx P_i\left(\mathbf{x}, \mathbf{x_0}, \omega\right)$. Rewriting equation 10 with $P'\left(\mathbf{x}, \mathbf{x_0}, \omega\right)$ substituted by $P_i\left(\mathbf{x}, \mathbf{x_0}, \omega\right)$,

$$P_s\left(\mathbf{x}, \mathbf{x_0}, \omega\right) \approx \int_{\mathbb{R}^3} \left(\mathbf{S}P_i\right)\left(\mathbf{x}', \mathbf{x_0}, \omega\right) \frac{e^{-j\frac{\omega}{c_0}\left|\mathbf{x}-\mathbf{x}'\right|}}{4\pi\left|\mathbf{x}-\mathbf{x}'\right|}\, d^3\mathbf{x}' \tag{11}$$

This approximation is referred to as the *(first) Born approximation* [7, 8, 9, 12, 13], and equation 11 states that the scattered pressure field is, to a first approximation, the spherically expanding wave $\frac{1}{4\pi\left|\mathbf{x}\right|}\exp\left(-j\frac{\omega}{c_0}\left|\mathbf{x}\right|\right)$ convolved onto the scattering term $\left(\mathbf{S}P_i\right)\left(\mathbf{x}, \mathbf{x_0}, \omega\right)$. If we regard the scatterers to be idealised points in $\mathcal{V}$, then this is equivalent to saying that these point scatterers each contribute a spherically expanding wave independently of each other. Thus, in making the Born approximation, we have implicitly assumed that multiply scattered waves (i.e. waves scattered off a particle that are then scattered off other particles) are negligible and that multiple scattering can be ignored [7, 9, 13].

By substituting the expression for $P_i(\mathbf{x}, \mathbf{x_0}, \omega)$ in equation 9 into equation 11, the scattered field can be expressed entirely in terms of the probe's characteristics and the scattering operator,

$$P_s\left(\mathbf{x}, \mathbf{x_0}, \omega\right) \approx j\omega\rho_0 V_n\left(\omega\right) \int_{\mathbb{R}^3} \left(\mathbf{S}H_s\right)\left(\mathbf{x}' - \mathbf{x_0}, \omega\right) \frac{e^{-j\frac{\omega}{c_0}\left|\mathbf{x}-\mathbf{x}'\right|}}{4\pi\left|\mathbf{x}-\mathbf{x}'\right|} d^3\mathbf{x}' \tag{12}$$

3.4 The Force on the Active Aperture

We recall from the physical description in section 2 that the received RF voltage trace is obtained by summing the scattered pressure field over the active aperture and filtering this sum by the electromechanical response of the piezoelectric crystals. In this subsection, we compute the summation of the scattered pressure field over the active aperture. Strictly speaking, this quantity, which will be denoted by $F(\mathbf{x_0}, \omega)$, is the force exerted on the active aperture [21].

Before we develop an expression for $F(\mathbf{x_0}, \omega)$, we introduce two lemmas that will be used in this subsection. The proofs for these lemmas are given in appendices A and B.

Lemma 1: For any vector-valued function $\mathbf{A}(\mathbf{x})$ and scalar function $b(\mathbf{x})$, if $\mathbf{A}(\mathbf{x})$ is zero outside some volume $\mathcal{V}'$, then

$$\int_{\mathcal{V}'} b(\mathbf{x}) \nabla \cdot \mathbf{A}(\mathbf{x}) \, d^3\mathbf{x} = -\int_{\mathcal{V}'} \mathbf{A}(\mathbf{x}) \cdot \nabla b(\mathbf{x}) \, d^3\mathbf{x} \tag{13}$$

Lemma 2: At locations that are far away from the active aperture,

$$(\nabla H_s \cdot \nabla H_s)(\mathbf{x}, \omega) \approx -\left(\frac{\omega}{c_0}\right)^2 H_s^2(\mathbf{x}, \omega) \tag{14}$$

Returning now to $F(\mathbf{x_0}, \omega)$, if we assume the same apodisation and focussing at reception as at transmission, then

$$F(\mathbf{x_0}, \omega) = \int_{\mathcal{A}} a_p(\mathbf{x_a}) \, e^{-j\omega\tau_d(\mathbf{x_a})} P_s(\mathbf{x_0} + \mathbf{x_a}, \mathbf{x_0}, \omega) \, d^2\mathbf{x_a} \tag{15}$$

Substituting in the integral expression for $P_s(\mathbf{x_0} + \mathbf{x_a}, \mathbf{x_0}, \omega)$ from equation 12 yields

$$\begin{aligned} F(\mathbf{x_0}, \omega) &\approx j\omega\rho_0 V_n(\omega) \int_{\mathcal{A}} a_p(\mathbf{x_a}) \, e^{-j\omega\tau_d(\mathbf{x_a})} \left[\int_{\mathbb{R}^3} \frac{(\mathbf{S}H_s)(\mathbf{x}' - \mathbf{x_0}, \omega) \, e^{-j\frac{\omega}{c_0}|\mathbf{x_0} + \mathbf{x_a} - \mathbf{x}'|}}{4\pi |\mathbf{x_0} + \mathbf{x_a} - \mathbf{x}'|} \, d^3\mathbf{x}' \right] d^2\mathbf{x_a} \\ &\approx j\omega\rho_0 V_n(\omega) \int_{\mathbb{R}^3} (\mathbf{S}H_s)(\mathbf{x}' - \mathbf{x_0}, \omega) \left[\int_{\mathcal{A}} \frac{a_p(\mathbf{x_a}) \, e^{-j\omega\tau_d(\mathbf{x_a})} \, e^{-j\frac{\omega}{c_0}|\mathbf{x_0} + \mathbf{x_a} - \mathbf{x}'|}}{4\pi |\mathbf{x_0} + \mathbf{x_a} - \mathbf{x}'|} \, d^2\mathbf{x_a} \right] d^3\mathbf{x}' \end{aligned} \tag{16}$$

We recognise from equation 8 that the integral in square brackets on the second line is equal to $\frac{1}{2} H_s(\mathbf{x}' - \mathbf{x_0}, \omega)$, and so

$$F(\mathbf{x_0}, \omega) \approx \frac{j\omega\rho_0 V_n(\omega)}{2} \int_{\mathbb{R}^3} (\mathbf{S}H_s)(\mathbf{x}' - \mathbf{x_0}, \omega) \, H_s(\mathbf{x}' - \mathbf{x_0}, \omega) \, d^3\mathbf{x}' \tag{17}$$

At this point, we substitute in the definition of the scattering operator $\mathbf{S}$ from equation 3,

$$F(\mathbf{x_0},\omega) \approx \frac{j\omega\rho_0 V_n(\omega)}{2}\left\{\left(\frac{\omega}{c_0}\right)^2 \int_{\mathbb{R}^3} \gamma(\mathbf{x}') H_s^2(\mathbf{x}'-\mathbf{x_0},\omega)\, d^3\mathbf{x}' - \int_{\mathbb{R}^3} \nabla\cdot[\mu(\mathbf{x}')(\nabla H_s)(\mathbf{x}'-\mathbf{x_0},\omega)] H_s(\mathbf{x}'-\mathbf{x_0},\omega)\, d^3\mathbf{x}'\right\} \tag{18}$$

To simplify the second integral on the RHS, we first note that $\mu(\mathbf{x})$ has finite support which allows us to apply equation 13 (lemma 1) to the second integral on the RHS,

$$F(\mathbf{x_0},\omega) \approx \frac{j\omega\rho_0 V_n(\omega)}{2}\left[\left(\frac{\omega}{c_0}\right)^2 \int_{\mathbb{R}^3} \gamma(\mathbf{x}') H_s^2(\mathbf{x}'-\mathbf{x_0},\omega)\, d^3\mathbf{x}' + \int_{\mathbb{R}^3} \mu(\mathbf{x}')(\nabla H_s\cdot\nabla H_s)(\mathbf{x}'-\mathbf{x_0},\omega)\, d^3\mathbf{x}'\right] \tag{19}$$

At sufficiently large distances away from the active aperture, we can use the approximation in equation 14 (lemma 2) to replace $(\nabla H_s\cdot\nabla H_s)$ with $-\left(\frac{\omega}{c_0}\right)^2 H_s^2$. This allows us to rewrite $F(\mathbf{x_0},\omega)$ as

$$F(\mathbf{x_0},\omega) \approx \frac{j\omega^3\rho_0 V_n(\omega)}{2c_0^2}\int_{\mathbb{R}^3} H_s^2(\mathbf{x}'-\mathbf{x_0},\omega)[\gamma(\mathbf{x}')-\mu(\mathbf{x}')]\, d^3\mathbf{x}' \tag{20}$$

What exactly is meant by 'sufficiently large distances away from the active aperture' is discussed in detail in appendix B. In short, equation 14 appears to be well satisfied at axial depths greater than the diameter of the active aperture [8]; for non-circular surfaces, this is the diameter of the smallest circle within which the active aperture can be inscribed.

It may be instructive to also consider equations 19 and 20 from the point-of-view of linear systems. We refer to figure 2(a), which illustrates graphically how the signal $F(\mathbf{x_0},\omega)$ is composed of monopole and dipole components (recall from subsection 3.1 that $\gamma(\mathbf{x})$ and $\mu(\mathbf{x})$ are monopole and dipole terms respectively). From a systems' point-of-view, $\gamma(\mathbf{x})$ and $\mu(\mathbf{x})$ are two distinct input signals, each convolved with a different spatiotemporal filter before being summed up and temporally filtered to produce $F(\mathbf{x_0},\omega)$. It is only at axial distances greater than the dimensions of the active aperture that the responses of the monopole and dipole spatiotemporal filters become sufficiently similar in magnitude for these input signals to be combined into a single input as shown in figure 2(b). In the special case that either of monopole or dipole scattering is dominant, one of the branches in the block diagram of figure 2(a) is effectively rendered negligible, and the linear system depicted in this block diagram is reduced to having just one input signal.

3.5 The RF Voltage Trace

We now model the electromechanical conversion of the force on the active aperture into a voltage trace. If we define the electromechanical transfer function that models this conversion to be $E_m(\omega)$ and the voltage trace to be $R(\mathbf{x_0},\omega)$, we have $R(\mathbf{x_0},\omega) = E_m(\omega)F(\mathbf{x_0},\omega)$ [9, 21]; substituting

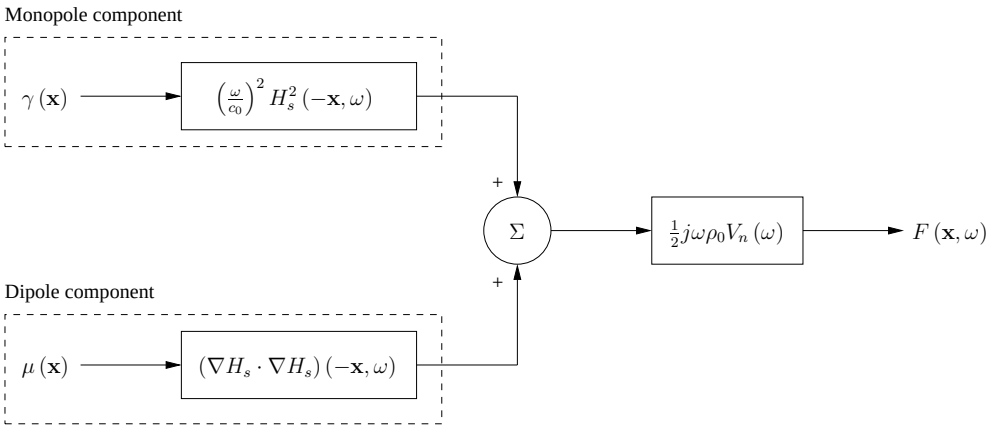

(a)

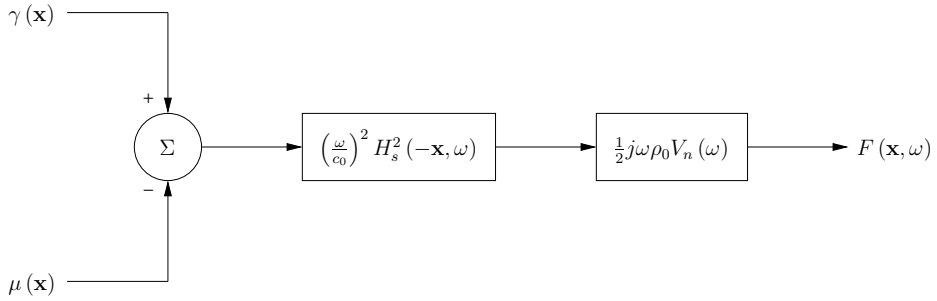

(b)

Figure 2: Block diagram representations of (a) equation 19 and (b) equation 20.

in the expression for $F(\mathbf{x_0},\omega)$ from equation 20,

$$R(\mathbf{x_0},\omega) \approx \frac{j\omega^3\rho_0 V_n(\omega) E_m(\omega)}{2c_0^2} \int_{\mathbb{R}^3} H_s^2(\mathbf{x}'-\mathbf{x_0},\omega)\left[\gamma(\mathbf{x}')-\mu(\mathbf{x}')\right] d^3\mathbf{x}' \tag{21}$$

For convenience, we group the properties of the medium together and the electromechanical characteristics of the probe together. We adopt definitions similar to those given in [9] and write the voltage trace as

$$R(\mathbf{x_0},\omega) \approx V_{pe}(\omega)\, H_s^2(-\mathbf{x},\omega) \underset{\mathbf{x}}{\otimes} f_m(\mathbf{x})\Big|_{\mathbf{x}=\mathbf{x_0}} \tag{22}$$

$$V_{pe}(\omega) = j\omega^3 V_n(\omega) E_m(\omega) \tag{23}$$

$$f_m(\mathbf{x}) = \frac{\rho_0^2\kappa_0}{2}\left[\frac{\Delta\kappa(\mathbf{x})}{\kappa_0} - \frac{\Delta\rho(\mathbf{x})}{\rho_0+\Delta\rho(\mathbf{x})}\right] \tag{24}$$

In keeping with the terminology introduced in [9], we refer to the quantities $V_{pe}(\omega)$ and $f_m(\mathbf{x})$ respectively as the *pulse-echo wavelet* and the *tissue reflectivity* or *scatterer field*. Note that to obtain the expression for $f_m(\mathbf{x})$ in equation 24, we have substituted in the definitions of c_0, $\gamma(\mathbf{x})$ and $\mu(\mathbf{x})$ from equations 1 and 4.

We can also express the voltage trace in the time domain as

$$r(\mathbf{x_0}, t) \approx v_{pe}(t) \underset{t}{\otimes} h_{pe}(-\mathbf{x}, t) \underset{\mathbf{x}}{\otimes} f_m(\mathbf{x}) \Big|_{\mathbf{x}=\mathbf{x_0}} \tag{25}$$

$$v_{pe}(t) = \mathcal{F}^{-1}\{V_{pe}(\omega)\} = -\frac{d^3 v_n}{dt^3}(t) \underset{t}{\otimes} e_m(t) \tag{26}$$

$$h_{pe}(\mathbf{x}, t) = \mathcal{F}^{-1}\left\{H_s^2(\mathbf{x}, \omega)\right\} \tag{27}$$

$$v_n(t) = \mathcal{F}^{-1}\{V_n(\omega)\} \tag{28}$$

$$e_m(t) = \mathcal{F}^{-1}\{E_m(\omega)\} \tag{29}$$

If we regard the quantity $f_m(\mathbf{x})$ as the input signal and $r(\mathbf{x_0}, t)$ as the output signal, equations 22 and 25 show very clearly that the imaging system is linear with a spatiotemporal transfer function $V_{pe}(\omega) H_s^2(-\mathbf{x}, \omega)$ or impulse response $v_{pe}(t) \underset{t}{\otimes} h_{pe}(-\mathbf{x}, t)$. Our definition of the transfer function of the imaging system in this way neatly distinguishes between the electromechanical characteristics of the probe (represented by the pulse-echo wavelet $V_{pe}(\omega)$) and the geometry of the probe (represented by the pulse-echo transfer function $H_s^2(\mathbf{x}, \omega)$).

4 Shift-Variance in the Axial Direction

To view ultrasound imaging from a purely signal processing point-of-view, we can combine the electromechanical response $v_{pe}(t)$ and the pulse-echo impulse response $h_{pe}(\mathbf{x}, t)$ into a single impulse response or PSF. If we formally define $h(\mathbf{x}, t) = v_{pe}(t) \underset{t}{\otimes} h_{pe}(\mathbf{x}, t)$, then

$$r(\mathbf{x_0}, t) \approx h(-\mathbf{x}, t) \underset{\mathbf{x}}{\otimes} f_m(\mathbf{x}) \Big|_{\mathbf{x}=\mathbf{x_0}} \tag{30}$$

We can gain a little more insight into the behaviour of the PSF by adopting the coordinate system shown in Figure 3, where the x, y and z axes are aligned with the lateral, elevational and axial directions respectively.

In a rectangular imaging system, a two-dimensional RF image is acquired by capturing RF traces at different lateral positions. A three-dimensional RF image is acquired by translating the probe in the elevational direction. Therefore, the vector $\mathbf{x_0}$ only changes laterally and elevationally, i.e. in the x and y directions only; its z coordinate never changes. Hence, without loss of generality, we can restrict the surface of the active aperture to lie on the xy plane. We can then write $\mathbf{x_0} = \begin{bmatrix} x & y & 0 \end{bmatrix}$ and $\mathbf{x} = \begin{bmatrix} x & y & z \end{bmatrix}$, and equation 30 can be written out in full as

$$r(x, y, t) \approx \int_{-\infty}^{+\infty}\!\!\!\!\!\!\iiint h(x' - x, y' - y, z', t)\, f_m(x', y', z')\, dx'\, dy'\, dz' \tag{31}$$

We see from equation 31 that the PSF is shift-variant along the axial direction but shift-invariant along the lateral and elevational directions.

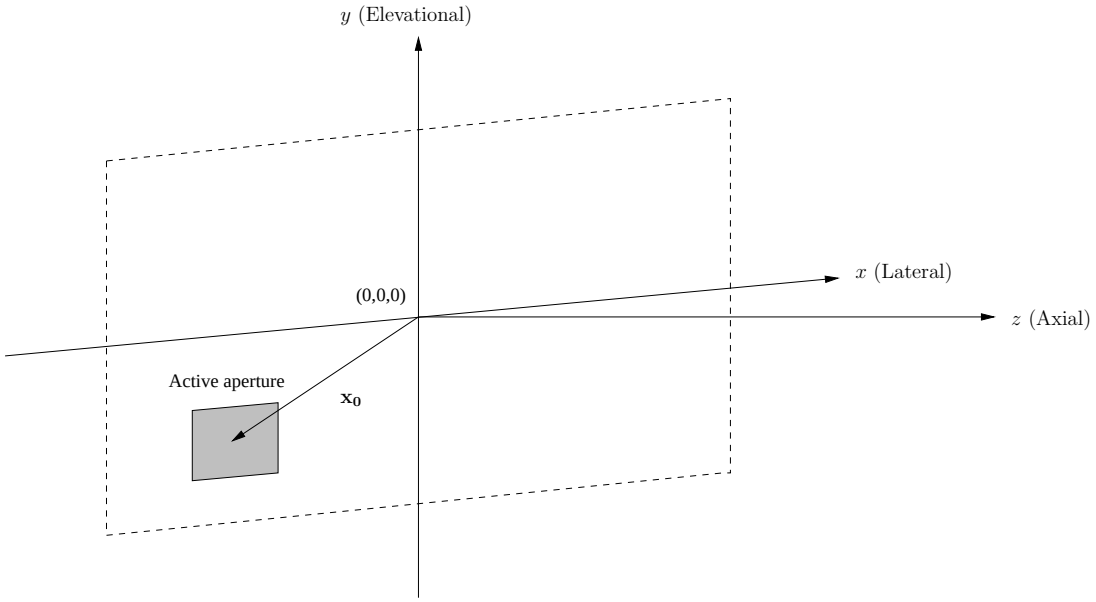

Figure 3: Coordinate system for demonstrating the shift-variance of the PSF in the axial direction.

An example of how a typical PSF varies with axial depth is given in Figure 4. This PSF was produced by simulating the response of a 6.5 MHz probe to ideal point scatterers at different axial depths. The probe contains 128 piezoelectric elements and the active aperture used to capture a single RF trace has 32 elements. Each element is 0.3 mm (lateral) by 6 mm (elevational) with a lateral gap of 0.1 mm between adjacent elements. The apodisation applied was a Hanning window. Both the lateral and elevational focal lengths were set to 20 mm. The simulation package used to carry out the simulation was Field II [10], which uses a discrete approximation to the Rayleigh integral to compute the spatial impulse response of the probe. The axial depths were calculated according to the approximation $z \approx \frac{1}{2}c_0 t$, where the value of c_0 was taken to be 1540 m/s (the factor of $\frac{1}{2}$ is needed because a pulse travels twice the axial depth in time t, from the probe to the scatterer and then back to the probe).

5 Complex Representation and Signal Statistics

Having derived an expression for $r(x, y, t)$ in terms of the point spread function and the scatterer field, most authors leave it there and cite one of the classic texts on speckle [6] when they wish to talk about the echo envelope amplitude of diffuse scattering as analogous to the distance travelled by a random walk in the complex plane. In this section we go through the algebra that links the real RF signal with the corresponding analytic representation in the complex plane. This enables us to make clear the assumptions that are involved, and also provides an explicit relationship between the envelope of the point spread function $h(x, y, z, t)$, and the statistics of fully developed speckle.

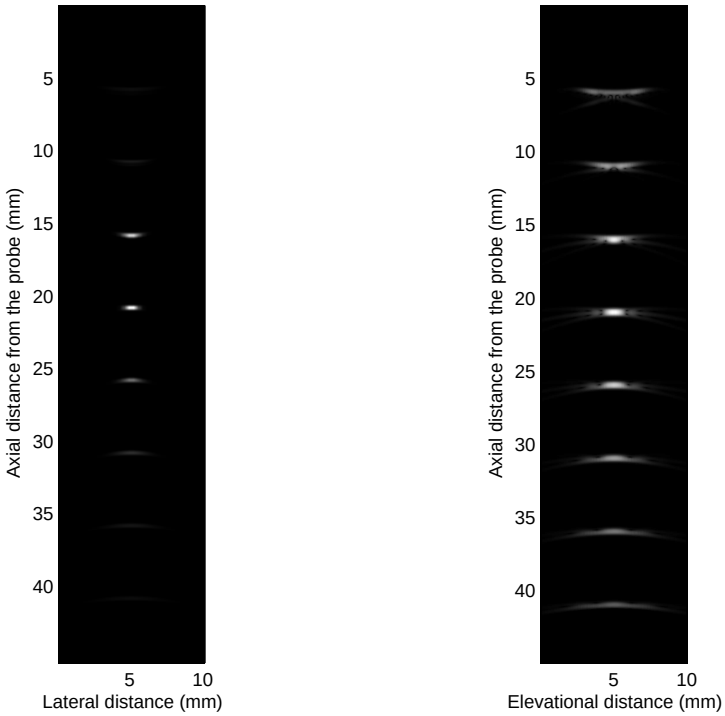

Figure 4: A typical system PSF at different axial depths from an apodised aperture after demodulation and logarithmic compression.

5.1 A Complex Baseband Model for RF Ultrasound

From equation (31) we have

$$r\left(x,y,t\right) \approx \iiint_{-\infty}^{+\infty} h\left(x'-x,y'-y,z',t\right) f_m\left(x',y',z'\right)\, dx'\; dy'\; dz'$$

We now form an analytic signal from the RF signal, using the Hilbert transform, $\mathcal{H}_t\{\bullet\}$ in the time dimension.

$$r(x,y,t) - j\mathcal{H}_t\{r(x,y,t)\} \approx \iiint_{-\infty}^{+\infty} \left[h\left(x'-x,y'-y,z',t\right) - j\mathcal{H}_t\{h\left(x'-x,y'-y,z',t\right)\}\right] f_m\left(x',y',z'\right)\, dx'\; dy'\; dz' \quad (32)$$

If we assume that the centre frequency of the RF ultrasound signal and the speed of sound in tissue are both reasonably constant we can define a representation for the complex analytic pulse in terms of its complex envelope, $\tilde{h}(x,y,z,t)$, the centre frequency ω_0 and centre wave number k_0.

$$h\left(x,y,z,t\right) - j\mathcal{H}_t\{h\left(x,y,z,t\right)\} = \tilde{h}(x,y,z,t)e^{j(\omega_0 t - 2k_0 z)} \quad (33)$$

See appendix C for a brief explanation of the factor of 2 in the exponent. Typically the centre frequency of an RF scan line varies by less than 5% in the z direction, and this variation can be accommodated by the complex envelope $\tilde{h}$, which we have assumed to be spatially varying in this direction.

We can therefore rewrite equation 32

$$\begin{aligned} & r(x,y,t) - j\mathcal{H}_t\{r(x,y,t)\} \\ & \qquad \approx \iiint_{-\infty}^{+\infty} \tilde{h}\left(x'-x, y'-y, z', t\right) e^{j\left(\omega_0 t - 2k_0 z'\right)} f_m\left(x', y', z'\right) dx'\ dy'\ dz' \\ & \qquad \approx e^{j\omega_0 t} \iiint_{-\infty}^{+\infty} \tilde{h}\left(x'-x, y'-y, z', t\right) f_m\left(x', y', z'\right) e^{-2jk_0 z'}\ dx'\ dy'\ dz' \end{aligned}$$

Hence

$$\left[r(x,y,t) - j\mathcal{H}_t\{r(x,y,t)\}\right] e^{-j\omega_0 t} \approx \iiint_{-\infty}^{+\infty} \tilde{h}\left(x'-x, y'-y, z', t\right) f_m\left(x', y', z'\right) e^{-2jk_0 z'}\ dx'\ dy'\ dz' \tag{34}$$

The left hand side of equation 34 is the analytic RF signal with the high frequency component at ω_0 removed. Let $\tilde{r}(x,y,t) = \left[r(x,y,t) - j\mathcal{H}_t\{r(x,y,t)\}\right] e^{-j\omega_0 t}$.

The term $f_m\left(x,y,z\right) e^{2jk_0 z}$ is made up of $f_m(x,y,z)$ which is a real function of position, and $e^{2jk_0 z}$ which determines the angle of the resulting complex number as a function of the remainder when the z position of the scatterer is divided by the wavelength, π/k_0, of the dominant frequency. For a 5 MHz probe this wavelength is roughly 0.3 mm, so we can assume that for diffuse scatterers the scatterer position is random within the wavelength. This means that the phase of the scatterer is effectively uniformly distributed in the range 0 to 2π. Let $\tilde{f}_m(x,y,z) = f_m\left(x,y,z\right) e^{-2jk_0 z}$, a vector with magnitude determined by $f_m(x,y,z)$ and random phase.

Thus we now have an analogous complex equation to the real equation (31) in which (a) the high frequency components have been removed by demodulating with the pulse centre frequency, (b) the pulse is now represented by a complex envelope analogous to the resolution cell of the imaging system and (c) the scatterers are represented by complex vectors of random phase.

$$\tilde{r}(x,y,t) \approx \iiint_{-\infty}^{+\infty} \tilde{h}\left(x'-x, y'-y, z', t\right) \tilde{f}_m\left(x', y', z'\right)\ dx'\ dy'\ dz' \tag{35}$$

where

$\tilde{r}(x,y,t)$ = $[r(x,y,t) - j\mathcal{H}_t\{r(x,y,t)\}]\, e^{-j\omega_0 t}$, the analytic RF signal with the $e^{j\omega_0 t}$ component removed

$\tilde{h}(x,y,z,t)$ = the complex envelope of the point spread function of the imaging system, i.e. the sensitivity to scatterers at the point (x,y,z) when forming the sum in $\tilde{r}$ for time t. Thus, this can also be viewed as the complex resolution cell or the complex pulse envelope relevant to the depth corresponding to time t.

$\tilde{f}_m(x,y,z)$ = the magnitude is from $f_m(x,y,z)$ and the phase from $e^{-2jk_0 z}$, so the phase is effectively random.

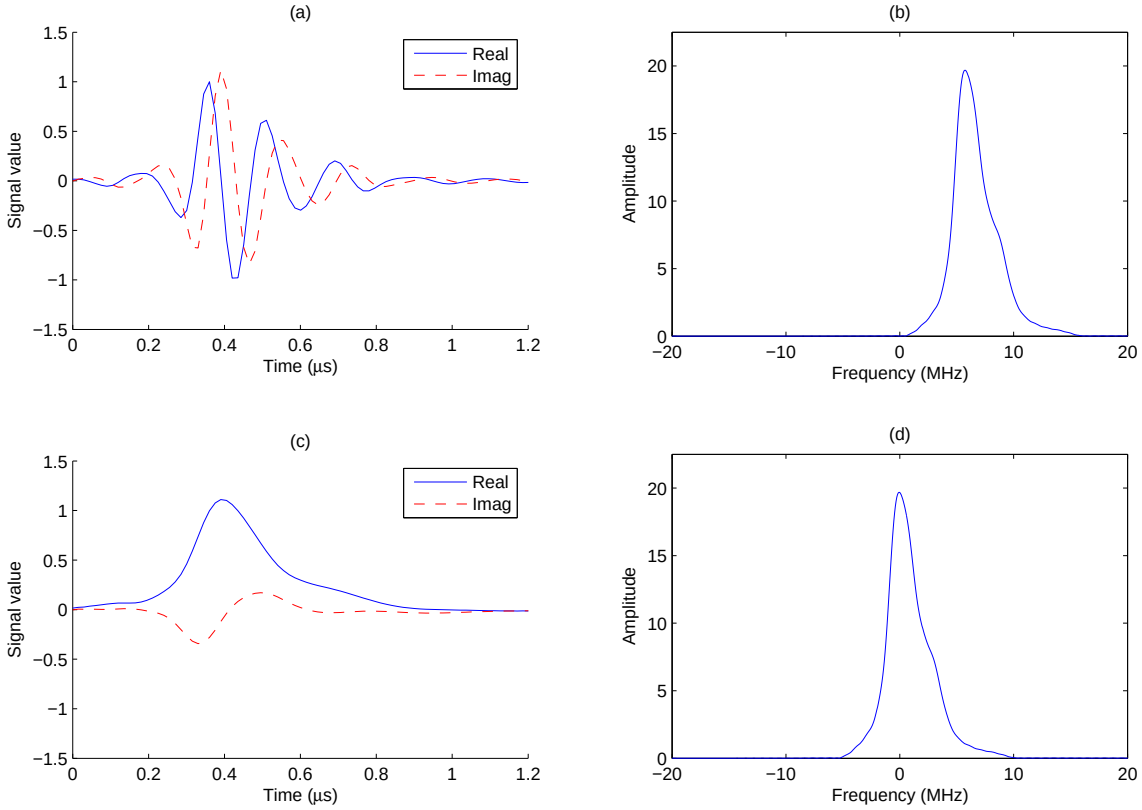

Figure 5: An analytic RF pulse de-rotated by its mode frequency of 5.79 MHz. (a) Real RF pulse and corresponding imaginary signal, computed using a Hilbert transform. (b) Amplitude spectrum of the pulse. (c) Pulse after multiplication by a sinusoid at 5.79 MHz. (d) Amplitude spectrum of (c). The vertical axes on all the graphs are in arbitrary units.

Note that we can calculate $\tilde{r}(x,y,t)$ from the measured RF signal, using an estimate of the pulse centre frequency. If we get the centre frequency slightly wrong this will have the effect of reducing the smoothness of $\tilde{h}(x,y,z,t)$. This is illustrated, using a simple example of an ultrasound pulse waveform, in figures 5 and 6. The analytic representation of the same pulse is shown in figures 5(a) and 6(a). In figure 5 the pulse is de-rotated by its mode frequency of 5.79 MHz, achieving a smooth envelope, which is shown in 5(c). Figure 6 shows that the asymmetry of the pulse's

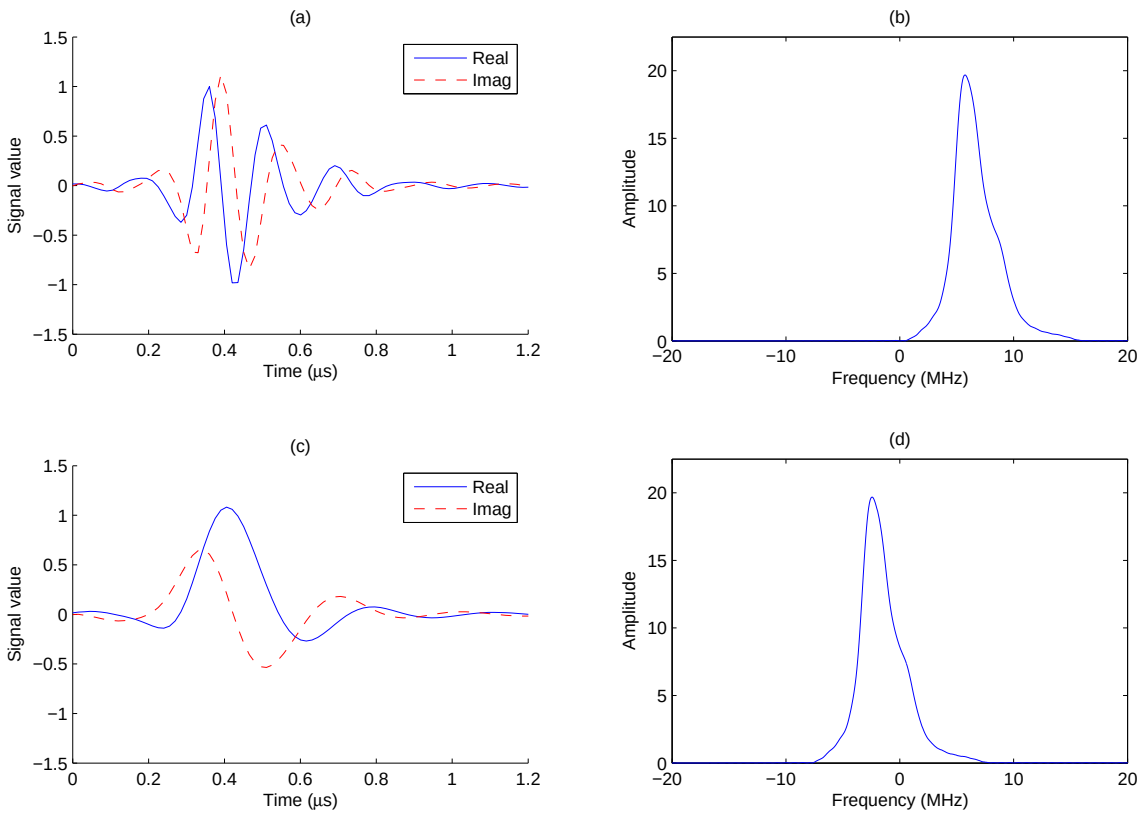

Figure 6: An analytic RF pulse de-rotated by its mean frequency of 8.17 MHz. (a) Real RF pulse and corresponding imaginary signal, computed using a Hilbert transform. (b) Amplitude spectrum of the pulse. (c) Pulse after multiplication by a sinusoid at 8.17 MHz. (d) Amplitude spectrum of (c). The vertical axes on all the graphs are in arbitrary units.

frequency histogram makes the mean frequency of 8.17 MHz less convenient to use for de-rotation in this case. Figure 6(c) shows a pulse envelope that is not as smooth as 5(c). Notice that in spite of the fact that there is a significant difference between 5.79 MHz and 8.17 MHz, the signal in 6(c) is still sufficiently smooth to be used as a plausible pulse envelope.

5.2 Statistics of Speckle

In all our discussion of speckle statistics we assume, without loss of generality, that we are working at a particular depth corresponding to the time t in the RF signal $\tilde{r}$.

From equation (35) we can see that each value in $\tilde{r}$ is formed from the sum of all the scatterers within the pulse envelope. Because of the $\tilde{f}_m$ term these scatterers have effectively random phase. If there are a large number of scatterers within the pulse envelope then, by the central limit theorem, the vector sum of these complex numbers will be distributed as a two-dimensional Gaussian

in the Argand diagram.

$$\mathbf{Pr}(\tilde{r}) = \frac{1}{2\pi\sigma^2} \exp\left[\frac{-\Re(\tilde{r})^2 - \Im(\tilde{r})^2}{2\sigma^2}\right]$$

where

$$\begin{aligned}
\mathbf{Pr}(\tilde{r}) &= \text{ the probability density function of } \tilde{r}. \\
\Re(\tilde{r}) &= \text{ the real part of } \tilde{r}. \\
\Im(\tilde{r}) &= \text{ the imaginary part of } \tilde{r}. \\
2\sigma^2 &= \langle f_m^2 \rangle \iiint_{-\infty}^{+\infty} \left[\tilde{h}(x,y,z,t)\right]^2 \, dx \; dy \; dz
\end{aligned}$$

$\langle \bullet \rangle$ denotes the expect value of a quantity. Note that the resolution cell $\tilde{h}$ varies with depth. We are taking the energy under the curve relevant to a depth given by time t in the RF signal. To find the amplitude distribution $|\tilde{r}\,|$, we express $\tilde{r}$ in polar coordinates and integrate over all angles.

$$\begin{aligned}
\tilde{r} &= \Re(\tilde{r}) + j\Im(\tilde{r}) = |\tilde{r}\,| e^{j\theta} \\
\Rightarrow \mathbf{Pr}(\tilde{r}) &= \frac{1}{2\pi\sigma^2} \exp\left(\frac{-|\tilde{r}\,|^2}{2\sigma^2}\right) \\
\Rightarrow \mathbf{Pr}(|\tilde{r}\,|) &= \int_0^{2\pi} \mathbf{Pr}(\tilde{r})\, d\theta = \frac{2\pi|\tilde{r}\,|}{2\pi\sigma^2} \exp\left(\frac{-|\tilde{r}\,|^2}{2\sigma^2}\right) \\
&= \frac{|\tilde{r}\,|}{\sigma^2} \exp\left(\frac{-|\tilde{r}\,|^2}{2\sigma^2}\right)
\end{aligned}$$

This gives us a Rayleigh distribution, as expected.

Now introduce variables to represent the amplitude and intensity of the backscattered signal.

$$\begin{aligned}
A &= |\tilde{r}\,| \qquad \text{(the amplitude)} \\
I &= A^2 \qquad \text{(the intensity)}
\end{aligned}$$

As already mentioned, the amplitude is Rayleigh distributed. The intensity follows an exponential distribution.

$$\begin{aligned}
\mathbf{Pr}(A) &= \frac{A}{\sigma^2} \exp\left(\frac{-A^2}{2\sigma^2}\right) \\
\mathbf{Pr}(I) &= \frac{1}{2\sigma^2} \exp\left(\frac{-I}{2\sigma^2}\right)
\end{aligned}$$

Also $\langle A \rangle = \sigma\sqrt{\frac{\pi}{2}}$, $\langle A^2 \rangle = \langle I \rangle = 2\sigma^2$ and $\langle I^2 \rangle = 8\sigma^4$.

5.3 Second Order Statistics of Speckle

Consider two points in space, labelled 1 and 2. They are located inside an ultrasound phantom that generates a fully developed speckle backscatter signal. Point 1 is at position (x_1, y_1, z_1) and

point 2 is at position $(x_1+\delta_x, y_1, z_1)$. Quantities at points 1 and 2 will be denoted using subscripts, for example A_1 is the amplitude at point 1.

Following equation 35 of [18], define λ as the magnitude of the normalised covariance of $\tilde{r}$

$$\lambda = \frac{|\langle \tilde{r}_1 \tilde{r}_2^* \rangle|}{2\sigma^2}$$

We assume that the resolution cell (point spread function) of the ultrasound scanner is an even function in the x direction: $\tilde{h}(x,y,z,t)$. Drawing on results from [14], as detailed in appendix D, we can directly obtain a convenient expression for λ in terms of the overlap of the resolution cells at points 1 and 2.

$$\lambda = 1 - \frac{\iiint_{-\infty}^{+\infty} \left[\tilde{h}(x+\delta_x,y,z,t) - \tilde{h}(x,y,z,t)\right]^2 \, dx \; dy \; dz}{2\iiint_{-\infty}^{+\infty} \left[\tilde{h}(x,y,z,t)\right]^2 \, dx \; dy \; dz} \tag{36}$$

The resolution cell $\tilde{h}$ varies slowly with depth determined by t. As $\tilde{h}$ does not generally extend over a wide range of z values for any particular value of t, this expression is valid at any depth provided $\tilde{h}$ is evaluated with the appropriate value of t.

If $\tilde{h}$ is a three dimensional Gaussian with standard deviation width in the x direction equal to w_x,

$$\tilde{h}(x,y,z,t) \propto \frac{1}{w_x w_y w_z (2\pi)^{\frac{3}{2}}} \exp\left[-\frac{x^2}{2w_x^2} - \frac{y^2}{2w_y^2} - \frac{\left(z - \frac{\omega t}{2k}\right)^2}{2w_z^2}\right]$$

then equation 36 evaluates to

$$\lambda^2 = \exp\left(\frac{-\delta_x^2}{2w_x^2}\right) \tag{37}$$

Note that the parameters of $\tilde{h}(x,y,z,t)$, i.e. w_x, w_y, k, ω and w_z will all vary slowly as a function of t.

From [11, 14, 17] the expected value of the products $I_1 I_2$ and $A_1 A_2$ are

$$\begin{aligned}
\langle I_1 I_2 \rangle &= 4\sigma^4 \left(1 + \lambda^2\right) \\
\langle A_1 A_2 \rangle &= \frac{\pi\sigma^2}{2} \, {}_2F_1\left(-\tfrac{1}{2}, -\tfrac{1}{2}; 1; \lambda^2\right) \\
&= \sigma^2 \left[2E(\lambda^2) - \left(1 - \lambda^2\right) K(\lambda^2)\right]
\end{aligned}$$

where ${}_2F_1(\bullet)$ is the Gaussian hypergeometric function [1, 11] and $K(\bullet)$ and $E(\bullet)$ are the complete elliptic integrals of the first and second kinds respectively. Following [1], we have adopted the convention that the arguments of $K(\bullet)$ and $E(\bullet)$ are given as the *parameter* (conventionally $K(m)$ and $E(m)$) rather than the *modulus* (conventionally $K(k)$ and $E(k)$ where $k^2 = m$). Other authors [11, 17], have chosen the alternate definition for these functions. Algorithms for evaluating the elliptic integrals are available in [1], and packages like Matlab (Mathworks Inc.) provide functions to compute them.

The Pearson correlation coefficient is defined

$$\rho(p,q) = \frac{\langle pq \rangle - \langle p \rangle \langle q \rangle}{\sqrt{\langle p^2 \rangle - \langle p \rangle^2}\sqrt{\langle q^2 \rangle - \langle q \rangle^2}} \tag{38}$$

Using equation (36) or (37) to determine λ, we can thus calculate the Pearson correlation coefficients of amplitude and intensity values separated by a distance δ_x in the x direction.

$$\rho(I_1, I_2) = \lambda^2 \tag{39}$$

$$\rho(A_1, A_2) = \frac{4E(\lambda^2) - 2\left(1-\lambda^2\right)K(\lambda^2) - \pi}{4-\pi} \tag{40}$$

If we assume that the complex resolution cell varies only slowly with depth, these formulae are valid for displacements in any direction, and not just in the x direction as described above.

Most of the results in subsections 5.2 and 5.3 are drawn from previous papers (eg. [3, 17]), but we believe equation 36, that relates λ to the overlap of the complex resolution cells, has not previously been published in this form.

6 Discussion and Conclusions

The major assumption underpinning this model is that of weak scattering; in our analysis, we showed that this means requiring the scattering to be weak enough that multiple scattering can be ignored. Most authors acknowledge that weak scattering occurs when the scatterers' acoustic properties differ from the medium's by small amounts [7, 9, 12], but overlook the fact that weak scattering also occurs when the size of the scatterers is very small compared to the wavelength of the incident wave, irrespective of the acoustic properties of the scatterers. At such small dimensions, the shape of the scatterers may be assumed to be spherical [16] and for a rigid sphere, the total power scattered is very small when the radius of the sphere is much less than $\frac{\lambda}{2\pi}$ [12, pp. 419–420].

In human tissue, the assumption of weak scattering does not hold at strongly reflecting interfaces such as organ boundaries. Cho *et al.* [5, p. 536], however, have suggested that it is possible to extend the linear model's validity beyond the Born approximation regime by modifying the PSF to account for some degree of multiple scattering.

The other significant limitation on our linear model is the approximation inherent in Equation 20. From a systems' point-of-view, the monopole and dipole terms $\gamma(\mathbf{x})$ and $\mu(\mathbf{x})$ are in fact two separate input signals contributing to the force on the active aperture (and therefore to the RF trace). The spatiotemporal filters applied by the physics of the system to each of these input signals are different; it is only at distances larger than the diameter of the transducer that the responses of these spatiotemporal filters become sufficiently similar (in magnitude) to allow $\gamma(\mathbf{x})$ and $\mu(\mathbf{x})$ to be combined into the single quantity $f_m(\mathbf{x})$. Of course, when one of the inputs is significantly larger than the other (i.e. when only one of monopole or dipole scattering is dominant), then we

may approximate this physical behaviour as a single-input, single-output linear system without this 'large distance' constraint.

We have shown how the expression for the RF signal in terms of the tissue reflectivity and a spatially varying PSF can be transformed into a representation in terms of complex analytic signals. The complex model incorporates a spatially varying complex PSF envelope that takes account of variations in the shape of the real PSF as well as well as changes in the speed of sound and the centre frequency of the backscattered signal.

It is easier to perform simulation and analysis of ultrasound scattering using this complex representation than using RF signals because accurate modelling of spatial variation on the scale of a wavelength is not necessary, and the various quantities do not vary at RF frequencies and hence can be sampled more sparsely. Our approach provides a direct interpretation of the complex quantities in terms of their RF analogues and thus makes it easier to understand the physical significance of results. We show how the complex representation can easily be used to derive the first and second order statistics of fully developed speckle.

Acknowledgements

James Ng is funded by Trinity College Cambridge. Graham Treece is funded by the Royal Academy of Engineering in association with the Engineering and Physical Sciences Research Council. The authors would like to thank Julian Sonner for helpful discussions on wave propagation and the solution of the wave equation.

List of Symbols

$\underset{t}{\otimes}$	Convolution with respect to t
$\underset{\mathbf{x}}{\otimes}$	Convolution with respect to $\mathbf{x}$
$\langle \bullet \rangle$	Expected value of a quantity
$\mathcal{A}$	Surface of the active aperture
A_1 and A_2	Amplitude of the signal at points 1 and 2
$a_p\left(\mathbf{x_a}\right)$	Apodisation weighting
c_0	Speed of sound in a homogeneous medium
$E_m\left(\omega\right)$ or $e_m\left(t\right)$	Electromechanical transfer function/impulse response
$E(\bullet)$	Complete elliptic integral of the second kind
$\mathcal{F}^{-1}\{\bullet\}$	Inverse temporal Fourier transform
$F\left(\mathbf{x_0}, \omega\right)$	Force on the active aperture
$f_m\left(\mathbf{x}\right)$ or $f_m\left(x, y, z\right)$	Tissue reflectivity
$\tilde{f}_m(x, y, z)$	Amplitude from tissue reflectivity, random phase
${}_2F_1(\bullet)$	Gaussian hypergeometric function

$h(\mathbf{x}, t)$ or $h(x, y, z, t)$	PSF of the imaging system
$h_{pe}(\mathbf{x}, t)$	Pulse-echo impulse response
$H_s(\mathbf{x}, \omega)$	Spatial transfer function
$\tilde{h}(x, y, z, t)$	Complex envelope of the point spread function
$\mathcal{H}_t\{\bullet\}$	Hilbert transform in time
$\Im(\bullet)$	Imaginary part of a number
I_1 and I_2	Intensity of signal at points 1 and 2
$K(\bullet)$	Complete elliptic integral of the first kind
k_0	Spatial frequency or wave number
$P'(\mathbf{x}, \omega)$	Total pressure field
$P_i(\mathbf{x}, \omega)$ or $P_i(\mathbf{x}, \mathbf{x_0}, \omega)$	Incident pressure field
$P_s(\mathbf{x}, \omega)$ or $P_s(\mathbf{x}, \mathbf{x_0}, \omega)$	Scattered pressure field
$\mathbf{Pr}(\bullet)$	Probability of a particular value
$\mathbb{R}^3$	Three-dimensional space
$R(\mathbf{x_0}, \omega)$ or $r(\mathbf{x_0}, t)$ or $r(x, y, t)$	RF Voltage trace
$\tilde{r}(x, y, t)$	Base-band analytic RF signal
$\Re(\bullet)$	Real part of a number
$\mathbf{S}$	Scattering operator
t	Time coordinate
$\mathcal{V}$	Volume containing scatterers
$V(\mathbf{x_a}, \omega)$	Position-dependent normal velocity over $\mathcal{A}$
$V_n(\omega)$ or $v_n(t)$	Position-independent normal velocity over $\mathcal{A}$
$V_{pe}(\omega)$ or $v_{pe}(t)$	Pulse-echo wavelet
w_x	Std. deviation width in x dir. of Gaussian resolution cell
$\mathbf{x}$	Position vector in three-dimensional space
$\mathbf{x}'$	Point in V; also a dummy variable of integration
$\mathbf{x_0}$	Centre of the active aperture
$\mathbf{x_a}$	Point on the active aperture
$\gamma(\mathbf{x})$	Compressibility (monopole) scattering term
$\Delta\kappa(\mathbf{x})$	Change in compressibility introduced by scatterers
$\Delta\rho(\mathbf{x})$	Change in density introduced by scatterers
δ_x	A small displacement in the x direction
κ_0	Uniform compressibility in a homogeneous medium
λ	Magnitude of normalised covariance of $\tilde{r}(x, y, z, t)$
$\mu(\mathbf{x})$	Density (dipole) scattering term
ρ_0	Uniform density in a homogeneous medium
$\rho(p, q)$	Pearson correlation coefficient between p and q
σ	Standard deviation of the probability distribution
$\tau_d(\mathbf{x_a})$	Delay term for focussing
ω	Temporal angular frequency

A Proof of Equation 13

For convenience, we restate equation 13:

> For any vector-valued function $\mathbf{A}(\mathbf{x})$ and scalar function $b(\mathbf{x})$, if $\mathbf{A}(\mathbf{x})$ is zero outside some volume $\mathcal{V}'$, then
>
> $$\int_{\mathcal{V}'} b(\mathbf{x}) \nabla \cdot \mathbf{A}(\mathbf{x}) \, d^3\mathbf{x} = -\int_{\mathcal{V}'} \mathbf{A}(\mathbf{x}) \cdot \nabla b(\mathbf{x}) \, d^3\mathbf{x}$$

Proof: This proof is taken from [12, pp. 325–326]. We begin with the identity

$$b(\mathbf{x}) \nabla \cdot \mathbf{A}(\mathbf{x}) = -\mathbf{A}(\mathbf{x}) \cdot \nabla b(\mathbf{x}) + \nabla \cdot [b(\mathbf{x}) \mathbf{A}(\mathbf{x})] \tag{41}$$

which can be verified by expanding the RHS and simplifying. Integrating both sides over $\mathcal{V}'$,

$$\int_{\mathcal{V}'} b(\mathbf{x}) \nabla \cdot \mathbf{A}(\mathbf{x}) \, d^3\mathbf{x} = -\int_{\mathcal{V}'} \mathbf{A}(\mathbf{x}) \cdot \nabla b(\mathbf{x}) \, d^3\mathbf{x} + \int_{\mathcal{V}'} \nabla \cdot [b(\mathbf{x}) \mathbf{A}(\mathbf{x})] \, d^3\mathbf{x} \tag{42}$$

By the divergence theorem [15, p. 407], the second integral on the RHS is equal to the surface integral $\oint_{\mathcal{S}'} b(\mathbf{x}) \mathbf{A}(\mathbf{x}) \cdot \hat{\mathbf{n}}(\mathbf{x}) \, d^2\mathbf{x}$, where $\mathcal{S}'$ is some surface enclosing $\mathcal{V}'$ and $\hat{\mathbf{n}}(\mathbf{x})$ is a unit vector normal to $\mathcal{S}'$. Since $\mathbf{A}(\mathbf{x})$ is zero outside $\mathcal{V}'$, the surface integral reduces to zero and equation 13 follows. Q.E.D.

B Proof of Equation 14

For convenience, we restate equation 14:

> At locations that are far away from the active aperture,
>
> $$(\nabla H_s \cdot \nabla H_s)(\mathbf{x}, \omega) \approx -\left(\frac{\omega}{c_0}\right)^2 H_s^2(\mathbf{x}, \omega)$$

Proof: We define the wave vector $\mathbf{k} = \frac{\omega}{c_0}\hat{\mathbf{r}}$, where $\hat{\mathbf{r}} = \frac{\mathbf{x}-\mathbf{x_a}}{|\mathbf{x}-\mathbf{x_a}|}$; in words, $\hat{\mathbf{r}}$ is a unit vector parallel to $\mathbf{x} - \mathbf{x_a}$ and $\mathbf{k}$ is a vector also parallel to $\mathbf{x} - \mathbf{x_a}$ but with magnitude $\frac{\omega}{c_0}$. We can then rewrite equation 8 for the spatial transfer function as

$$H_s(\mathbf{x}, \omega) = \frac{1}{2\pi} \int_{\mathcal{A}} a_p(\mathbf{x_a}) \, e^{-j\omega\tau_d(\mathbf{x_a})} \, \frac{e^{-j\mathbf{k}\cdot(\mathbf{x}-\mathbf{x_a})}}{|\mathbf{x} - \mathbf{x_a}|} \, d^2\mathbf{x_a} \tag{43}$$

Taking the gradient,

$$\begin{aligned}
(\nabla H_s)(\mathbf{x},\omega) &= \frac{1}{2\pi}\int_{\mathcal{A}} a_p(\mathbf{x_a})\, e^{-j\omega\tau_d(\mathbf{x_a})} \nabla\left[\frac{e^{-j\mathbf{k}\cdot(\mathbf{x}-\mathbf{x_a})}}{|\mathbf{x}-\mathbf{x_a}|}\right] d^2\mathbf{x_a} \\
&= \frac{1}{2\pi}\int_{\mathcal{A}} a_p(\mathbf{x_a})\, e^{-j\omega\tau_d(\mathbf{x_a})} \left[\frac{\nabla e^{-j\mathbf{k}\cdot(\mathbf{x}-\mathbf{x_a})}}{|\mathbf{x}-\mathbf{x_a}|} + e^{-j\mathbf{k}\cdot(\mathbf{x}-\mathbf{x_a})}\nabla\left(\frac{1}{|\mathbf{x}-\mathbf{x_a}|}\right)\right] d^2\mathbf{x_a} \\
&= \frac{1}{2\pi}\int_{\mathcal{A}} a_p(\mathbf{x_a})\, e^{-j\omega\tau_d(\mathbf{x_a})} \left[-j\mathbf{k}\,\frac{e^{-j\mathbf{k}\cdot(\mathbf{x}-\mathbf{x_a})}}{|\mathbf{x}-\mathbf{x_a}|} - \frac{e^{-j\mathbf{k}\cdot(\mathbf{x}-\mathbf{x_a})}}{|\mathbf{x}-\mathbf{x_a}|^2}\,\hat{\mathbf{r}}\right] d^2\mathbf{x_a} \\
&= \frac{1}{2\pi}\int_{\mathcal{A}} a_p(\mathbf{x_a})\, e^{-j\omega\tau_d(\mathbf{x_a})} \frac{e^{-j\mathbf{k}\cdot(\mathbf{x}-\mathbf{x_a})}}{|\mathbf{x}-\mathbf{x_a}|}\left(-j\mathbf{k} - \frac{\hat{\mathbf{r}}}{|\mathbf{x}-\mathbf{x_a}|}\right) d^2\mathbf{x_a} \qquad (44)
\end{aligned}$$

We apply the condition $\frac{1}{|\mathbf{x}-\mathbf{x_a}|} \ll |\mathbf{k}| = \frac{\omega}{c_0}$, which is equivalent to $|\mathbf{x}-\mathbf{x_a}| \gg \frac{\lambda}{2\pi}$ since $\frac{\omega}{c_0} = \frac{2\pi}{\lambda}$. Equation 44 then reduces to

$$(\nabla H_s)(\mathbf{x},\omega) \approx \frac{1}{2\pi}\int_{\mathcal{A}} a_p(\mathbf{x_a})\, e^{-j\omega\tau_d(\mathbf{x_a})} \frac{e^{-j\mathbf{k}\cdot(\mathbf{x}-\mathbf{x_a})}}{|\mathbf{x}-\mathbf{x_a}|}(-j\mathbf{k})\, d^2\mathbf{x_a} \qquad (45)$$

We also assume that the direction of $\mathbf{k}$ does not vary very much over the active aperture which allows the $-j\mathbf{k}$ term on the RHS to be factored out of the integral,

$$(\nabla H_s)(\mathbf{x},\omega) \approx \frac{-j\mathbf{k}}{2\pi}\int_{\mathcal{A}} a_p(\mathbf{x_a})\, e^{-j\omega\tau_d(\mathbf{x_a})} \frac{e^{-j\mathbf{k}\cdot(\mathbf{x}-\mathbf{x_a})}}{|\mathbf{x}-\mathbf{x_a}|} d^2\mathbf{x_a} = -j\mathbf{k}\, H_s(\mathbf{x},\omega) \qquad (46)$$

Equation 14 follows from this immediately. Q.E.D.

In practice, the condition $|\mathbf{x}-\mathbf{x_a}| \gg \frac{\lambda}{2\pi}$ is satisfied for virtually the entire imaged region, since the wavelengths from medical ultrasound probes are usually very short. For example, consider a typical probe transmitting at 6.5 MHz into human tissue which has an average speed of sound of 1540 m/s. For this probe, $\frac{\lambda}{2\pi} = 0.0377$ mm which is practically negligible.

The condition that the direction of $\mathbf{k}$ not vary very much over the active aperture is much stricter and is only satisfied in regions far away from the active aperture. To quantify exactly what is meant by 'far away', we consider the setup of Figure 7.

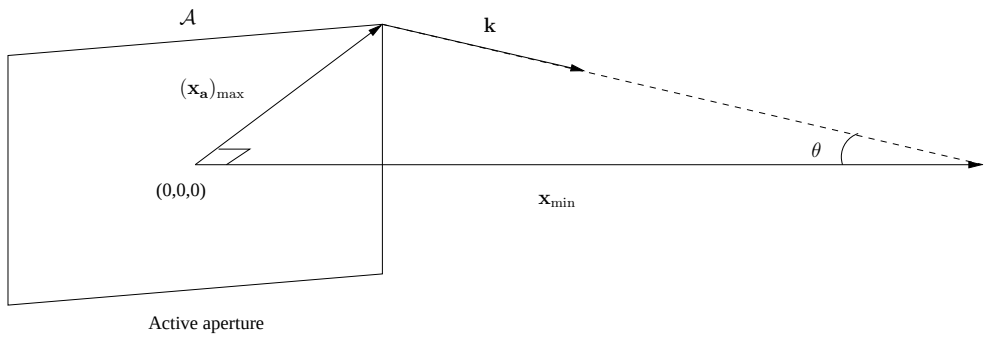

Figure 7: Coordinate system for calculating an approximation to $(\nabla H_s \cdot \nabla H_s)(\mathbf{x},\omega)$.

For a typical focussed probe, we expect the majority of the transmitted acoustic energy to be concentrated in a small region enclosing the axial axis, and so we have chosen to consider only the scenario where $\mathbf{x}$ lies along this axis. We can restate our requirement that $\mathbf{k}$ be uniform over the active aperture by equivalently requiring $\mathbf{k}$ to be approximately parallel to $\mathbf{x}$.

This requirement is most difficult to satisfy when we consider the point on the active aperture farthest from the active aperture's centre, i.e. when $\mathbf{x_a} = (\mathbf{x_a})_{\max}$. Our requirement that $\mathbf{k}$ be approximately parallel to $\mathbf{x}$ can be stated in terms of the dot product as $\mathbf{k} \cdot \mathbf{x} \approx |\mathbf{k}|\,|\mathbf{x}|$; in the case where $\mathbf{x_a} = (\mathbf{x_a})_{\max}$ (as shown in Figure 7), we require $\cos\theta \approx 1$. If we allow a 10% error in this approximation for $\cos\theta$, we effectively impose the constraint $\cos\theta > 0.9 \Rightarrow \theta < 26°$. From Figure 7, $|\mathbf{x}_{\min}| = |(\mathbf{x_a})_{\max}| \cot\theta$ and so our requirement that $\theta < 26°$ translates to requiring $|\mathbf{x}| > 2\,|(\mathbf{x_a})_{\max}|$.

What we have demonstrated in this brief discussion is that the approximation in equation 14 is satisfied well at axial depths that are greater than the diameter of the active aperture (for non-circular apertures, this diameter is the diameter of the smallest circle within which the active aperture can be inscribed). The same claim is made without proof in [8].

C Motivation for Equation 33

Consider a pulse P of an unspecified complex quantity propagating into a medium in the z direction at speed ω/k.

$$P\left(\omega t - kz\right)$$

It is reflected at a depth z_1 and travels back in the $-z$ direction. Changes in phase and amplitude during the reflection are represented by q_1. The reflected pulse is

$$q_1 P\left(\omega t + \left(z - z_1\right)k - z_1 k\right)$$

When this pulse gets back to the probe, i.e. $z = 0$, we have

$$q_1 P\left(\omega t - 2kz_1\right)$$

Hence we represent $h\left(x, y, z, t\right) - j\mathcal{H}_t\{h\left(x, y, z, t\right)\}$ as $\tilde{h}(x, y, z, t)e^{j(\omega_0 t - 2k_0 z)}$ in equation 33.

D Proof of Equation 36

We start by reproducing equation 35 from [18] in our notation, and introduce a modulus sign as the analytic signal can otherwise result in a complex value (as noted in the comment below equation 36 in [18]).

$$\lambda = \frac{|\langle \tilde{r}_1 \tilde{r}_2^* \rangle|}{2\sigma^2}$$

Using equation 18 from [17] together with the definition of the Pearson correlation coefficient (equation 38), we can compute equation 39 in the main text of this paper.

$$\rho(I_1, I_2) = \lambda^2 \tag{47}$$

Equation A.6 in [14] is

$$\rho(I_1, I_2) = b \tag{48}$$

(the reader is referred to [14] for the definition of b) and equation 14 from [14] is

$$b = \left(1 - \frac{\langle i \rangle}{\langle I \rangle}\right)^2 \tag{49}$$

Combining equations 47, 48 and 49 gives us

$$\lambda = 1 - \frac{\langle i \rangle}{\langle I \rangle} \tag{50}$$

The quantities $\langle i \rangle$ and $\langle I \rangle$, which are defined in [14], can be expressed in terms of the complex resolution cell $\tilde{h}$ using equations 21 and 22 from that paper.

$$\langle I \rangle = k^2 \iiint_{-\infty}^{+\infty} \left[\tilde{h}(x,y,z,t)\right]^2 \, dx \; dy \; dz$$

$$\langle i \rangle = \frac{1}{2} k^2 \iiint_{-\infty}^{+\infty} \left[\tilde{h}(x+\delta_x,y,z,t) - \tilde{h}(x,y,z,t)\right]^2 \, dx \; dy \; dz$$

where k^2 represents the average backscattering intensity. We can substitute these expressions into equation 50 and cancel k^2, to give equation 36

$$\lambda = 1 - \frac{\iiint_{-\infty}^{+\infty} \left[\tilde{h}(x+\delta_x,y,z,t) - \tilde{h}(x,y,z,t)\right]^2 \, dx \; dy \; dz}{2 \iiint_{-\infty}^{+\infty} \left[\tilde{h}(x,y,z,t)\right]^2 \, dx \; dy \; dz}$$

References

[1] M. Abramowitz and I. A. Stegun. *Handbook of mathematical functions.* Dover, 1970.

[2] Martin E. Anderson and Gregg E. Trahey. A seminar on k-space applied to medical ultrasound. Technical report, Department of Biomedical Engineering, Duke University, April 2000. Available: http://dukemil.egr.duke.edu/Ultrasound/k-space/bme265.htm [2004, December 15].

[3] C. B. Burckhardt. Speckle in ultrasound B-mode scans. *IEEE Transactions on Sonics and Ultrasonics*, SU-25(1):1–6, January 1978.

[4] George F. Carrier and Carl E. Pearson. *Partial Differential Equations: Theory and Technique.* Academic Press, 1976.

[5] Zang-Hee Cho, Joie P. Jones, and Manbir Singh. *Foundations of Medical Imaging.* John Wiley and Sons, 1993.

[6] J.W. Goodman. Statistical properties of laser speckle patterns. In J.C. Dainty, editor, *Laser Speckle and Related Phenomena*, pages 9–75. Springer-Verlag, 1975.

[7] J.C. Gore and S. Leeman. Ultrasonic backscattering from human tissue: a realistic model. *Physics in Medicine and Biology*, 22(2):317–326, 1977.

[8] Michael F. Insana, Robert F. Wagner, David G. Brown, and Timothy J. Hall. Describing small-scale structure in random media using pulse-echo ultrasound. *Journal of the Acoustical Society of America*, 87(1):179–192, January 1990.

[9] Jorgen Arendt Jensen. A model for the propagation and scattering of ultrasound in tissue. *Journal of the Acoustical Society of America*, 89(1):182–190, January 1991.

[10] Jorgen Arendt Jensen. Field: a program for simulating ultrasound systems. In *Proceedings of the 10th Nordic-Baltic Conference on Biomedical Imaging, Medical and Biological Engineering and Computing in Tampere*, volume 34, pages 351–353, 1996.

[11] D. Middleton. *An Introduction to Statistical Communication Theory.* McGraw-Hill, 1960.

[12] Philip M. Morse and K. Uno Ingard. *Theoretical Acoustics.* McGraw-Hill Book Company, 1968.

[13] Allan D. Pierce. *Acoustics: An Introduction to Its Physical Principles and Applications.* McGraw-Hill Series in Mechanical Engineering. McGraw-Hill Book Company, 1981.

[14] R. W. Prager, A. H. Gee, G. M. Treece, C. J. C. Cash, and L. H. Berman. Sensorless freehand 3D ultrasound using regression of the echo intensity. *Ultrasound in Medicine and Biology*, 29(3):437–446, March 2003.

[15] K.F. Riley, M.P. Hobson, and S.J. Bence. *Mathematical Methods for Physics and Engineering.* Cambridge University Press, second edition, 2002.

[16] V.A. Shutilov. *Fundamental Physics of Ultrasound.* Gordon and Breach, 1988.

[17] R. F. Wagner, S. W. Smith, J. M. Sandrik, and H. Lopez. Statistics of speckle in ultrasound B-scans. *IEEE Transactions on Sonics and Ultrasonics*, 30(3):156–163, May 1983.

[18] R.F. Wagner, M. F. Insana, and D. G. Brown. Statistical properties of radio-frequency and envelope-detected signals with applications to medical ultrasound. *Journal of the Optical Society of America A*, 4(5):910–922, May 1987.

[19] K. A. Wear, R.F. Wagner, and D. G. Brown. Statistical properties of estimates of signal-to-noise ratio and number of scatterers per resolution cell. *Journal of the Acoustical Society of America*, 102(1):635–641, July 1997.

[20] P. N. T. Wells and M. Halliwell. Speckle in ultrasonic imaging. *Ultrasonics*, 19(5):225–229, September 1981.

[21] Roger J. Zemp, Craig K. Abbey, and Michael F. Insana. Linear system models for ultrasonic imaging: application to signal statistics. *IEEE Transactions on Ultrasonics, Ferroelectrics and Frequency Control*, 50(6):642–654, June 2003.

[22] Lawrence J. Ziomek. *Fundamentals of Acoustic Field Theory and Space-Time Signal Processing*. CRC Press, 1995.